

# Impact of spatially varying flow conditions on the prediction of fatigue loads of a tidal turbine

Hannah R. Mullings and Tim Stallard

**Abstract**—Site development for tidal turbines relies upon a good understanding of the onset flow conditions, with disk averaged velocity typically used as a reference to define turbine power and mean loading. This work investigates the variation of onset flow conditions which occur for the same disk averaged velocity. Analysis builds upon data previously acquired during the measurement campaign conducted for the ReDAPT project using bed mounted ADCPs [1]. These measurements define the turbulence characteristics and vertical shear profiles over the rotor plane which are incorporated into an efficient blade element method for prediction of unsteady blade loads. This method allows efficient calculation of blade loading for multiple onset shear and turbulence profiles, each with the same disk average velocity, to determine the cyclic loading which contributes towards fatigue. Predictions of fatigue loads from measured profiles are compared with predictions from profiles predicted for the same location with a MIKE3 model [2]. Within the water depth two vertical positions are analysed, with vertical shear profiles from measurements and a multi-parameter model used to define the onset. For a near-bed location, use of the averaged predicted velocity profiles neglecting variation of turbulence intensity with flow-speed provides fatigue loads to within 1% of predictions obtained using all measured profiles of velocity and corresponding turbulence intensity. For the near-surface location, the same approach under predicts fatigue loads by 16-19%. This is partly due to the occurrence of a wider range of turbulence intensities. Since this is nearly constant with flow-speed a scaling factor is applied to load cycles from predicted profiles to estimate the aggregated fatigue load obtained using all measured conditions, providing confidence that accumulated fatigue loads can be predicted efficiently from velocity profiles obtained from shallow water models.

**Index Terms**—Blade Loading, Spatial Variation, Tidal Turbine.

## I. INTRODUCTION

**T**O further the development of tidal turbines as a suitable choice for energy generation in large

Manuscript received December 30th, 2021, published 10 June 2022.

This is an open access article distributed under the terms of the Creative Commons Attribution 4.0 licence (CC BY <http://creativecommons.org/licenses/by/4.0/>). Unrestricted use (including commercial), distribution and reproduction is permitted provided that credit is given to the original author(s) of the work, including a URI or hyperlink to the work, this public license and a copyright notice. This article has been subject to single-blind peer review by a minimum of two reviewers.

This work was supported by the Tidal Stream Industry Energiser Project (TIGER), co-funded by the European Regional Development Fund through Interreg France Channel Programme.

H. R. Mullings is at The University of Manchester, Oxford Road, Manchester, M13 9PL (e-mail: hannah.mullings@manchester.ac.uk).

T. Stallard is at The University of Manchester, Oxford Road, Manchester, M13 9PL (e-mail: tim.stallard@manchester.ac.uk).

Digital Object Identifier: <https://doi.org/10.36688/imej.5.103-111>

arrays spatial variation in tidal site conditions should be understood. Currently design standards [3], [4] stipulate that current measurements for establishing tidal turbine conditions can be located 1-5 turbine diameters from the turbine, depending on the alignment to the oncoming flow. This study aims to establish the dependency of turbine fatigue loads on the onset conditions (velocity and turbulence) obtained from a shallow-water model and from site measurements. A point two diameters adjacent to a turbine location is considered as per the design standard. Site data used is from the ReDAPT project, with pre-processing of the data conducted at the University of Edinburgh [5], [1]. This data has been used in numerous studies into modelling the power curve of a full scale turbine [6], validating loads and performance [7] as well as the characterisation of tidal flows [1]. The data has enabled the comparison and validation of computational models to determine the hydrodynamic loads on the turbine. In this work an efficient blade element method will be used to determine the unsteady loading experienced by a turbine at two different turbine heights for three different performance points. Previous work by Sellar et al. [1] describes the deployments in detail and gives the ADCP locations relative to the turbine. This work focuses on one ADCP which was deployed between September and December in 2014 at an approximate depth of 43 m.

Spatial variation of turbines within a chosen site has the primary aim of the best locations for power capture. To specify the conditions at a site previous measurement campaigns are conducted to allow for model comparisons. This work will compare the uncertainty in load prediction due to the method used to give the unsteady conditions. Using the site measurements two different turbine height positions are investigated to represent a bed mounted and a 'floating' turbine. The turbine modelled in this case uses the blade data available from TGL/Alstom turbine as the reference turbine. Unsteady loading conditions are considered here through the use of measured and predicted shear profiles. With fatigue loading determined through the use of a blade element method to inform load cycles, hence the damage equivalent loads. Fatigue loads due to environmental conditions have been examined for example by [8], [9], [7] using damage equivalent loads. This method is suitable to calculate Fatigue according to the DNV-GL Standard [3]. These loads are determined using Tidal Bladed [8], [9] with [7] also using this software but including a comparison to loads on

a full scale device. Firstly, the aim is to assess the influence of the modelling approach on the predicted fatigue loads relative to the measured profiles. Secondly to evaluate the impact of the turbine position.

## II. SITE AND SYSTEM CHARACTERISTICS

This work utilised data gathered as part of the ReDAPT project. This section describes key aspects of the onset flow and the system considered. The data obtained in the ReDAPT project gathered velocity measurements from bed mounted ADCPs for a concurrent period of time. In this study, data from one ADCP is used for a period of 70 days, which includes 5 tidal cycles in order to examine the load cycles over a representative period. In this study the interest is in understanding the different disk averaged velocity considered as the onset flow ( $U_{DA}$ ) to the turbine. Previous work using the site data from the ReDAPT project established the power curve [10]. Based upon this curve three velocity bins have been chosen to examine the variation in onset flow conditions, with these velocity bands representing a point below rated power, at rated power and above.

### A. Onset flow characteristics

Data provided by ADCPs allows a vertical profiles of velocity to be determined. Table I defines the device information for the ADCP used in this work from the ReDAPT project.

TABLE I  
DEVICE INFORMATION FROM THE RDI WORKHORSE USED IN THE  
REDAPT PROJECT [11].

Device	
Bin Size (m)	1
Sample Rate (Hz)	0.5
Initial Bin Height (m)	3.1
Latitude (deg)	59.1370
Latitude (deg)	-2.805

Following the design standards [3] a 10 minute average is used in this work to identify the range of onset flow speeds. The onset flow conditions studied here are defined from the ADCP data. With the top turbine at a hub height of 28 m from the bed and the bed mounted turbine with a hub height of 15 m from the bed. The onset flow condition experienced by the turbine is calculated using the power weighted average across the rotor plane. The standard choice is to use a rotor-disk averaged velocity to describe a steady-state case. In this work the rotor-disk averages ( $U_{DA}$ ) are determined for the two different vertical positions, these disk averages are calculated using a vertical strip wise method, as described in [10]. Where the measured velocity from the ADCP at different vertical positions down the rotor plane, are then averaged over the rotor plane using Equation 1, with more detail into the rotor segments shown in Figure 1.

$$U_{DA} = \left[ \frac{1}{A_D} \sum_{i=1}^n U_i^3(z) A_i \right]^{1/3} \quad (1)$$

Where  $A_D$  is the rotor area,  $U_i(z)$  is the velocity at each vertical velocity bin and  $A_i$  is the strip wise area of each bin.

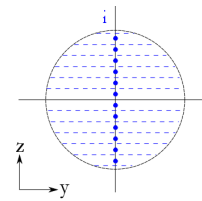


Fig. 1. Rotor disk area, segmented for use with a vertical velocity profile

Using the 10 minute intervals where the  $U_{DA}$  falls between each velocity bin the fluctuation intensity is determined at the hub height of each rotor. The fluctuation intensity is determined using Equation 2, which is usually used to determine the turbulence intensity.

$$I = \frac{u'}{\bar{u}} \quad (2)$$

Where  $\bar{u}$  is the mean velocity and  $u'$  is the root-mean-square of the velocity fluctuations. In this work the intensity calculated is described and used only as the fluctuation intensity. This is due to the ADCP measurements capturing the variation in velocity due to waves as well as turbulence. The ADCP measurements are also used to define the turbulence lengthscales. The calculation of turbulence lengthscales utilises the 10 minute intervals of onset flow data which fall between different velocity bins. For each hub height a number of samples are extracted, the lengthscales are calculated at the hub height for each turbine position through the use of an auto-correlation function.

### B. Turbine Characteristics

During the ReDAPT project, Alstom Energy's DEEP-Gen IV 1 MW tidal turbine was deployed at the EMEC test facility. Geometry representative of this turbine is used in this work. A turbine of 18 m diameter is located at both positions investigated, in reality a floating turbine may be required to have a smaller diameter than a bed mounted turbine for the same size due to constraints of the free surface. With varying disk averaged velocities determined and binned the rotational speed of the turbine for each load case will vary allowing a constant tip-speed-ratio (TSR) to be achieved.

## III. METHOD

There are many different methods to calculate the loading experienced on a tidal turbine. Computationally these methods range from expensive modelling of the complete turbine blade to quicker methods which produce overall turbine loading characteristics. One of the quicker methods is to use blade-element momentum (BEM) theory which is a numerical method utilising actuator disk theory. This method has been validated as a tool to predict wind and tidal turbine performance, and is fully utilised in the commercial

TABLE II  
SET UP FOR DIFFERENT CASES IN ORDER TO EXAMINE THE VARIATION IN LOAD FROM EACH CASE.

Cases	Shear Profile			Turbulence		
	None	Varying	Average	Estimated	Varying	Constant
A		✓			✓	
B		✓				✓
C			✓		✓	
D			✓			✓

software Tidal Bladed. Another method that can be used is computational fluid dynamics (CFD) which enables the calculation of loads through the creation of actuator disk [12], actuator line [13] and fully-blade resolved models [14]. These models increase in complexity and computational cost, in some cases they are not practical to use to determine long term loading or array configurations.

This work draws upon an efficient blade element method which draws upon onset flow data from a frozen turbulence model. Previous work has shown peak shear loading can be predicted to within 1% of an experimental load spectra for root bending moment [15] with fatigue loads predicted to within 7% of the experimental value [16], when the von Karman method is used to generate the frozen turbulence field.

The characteristics which inform this model have been determined from the ADCP measurements and predicted from models. For multiple flow speed ranges the differences in onset flow conditions is investigated. Using the measured case, a range of shear profiles are found as well as the fluctuation intensity and integral turbulence lengthscales. Using the calculated disk average velocities predicted shear profiles have been determined to compare the variation in load. For one flow speed case the load variation between turbine locations is determined. Table II explains the choice of profiles to compare the differences in loading for the same  $U_{DA}$ .

#### A. Blade Loading

After determining the inflow to the turbine using a turbulent domain, and any additional onset flow conditions, the loading can be established. The method employed here extracts the onset flow at  $N$  positions along a blade length, which rotate with time, depending on the chosen operating point. The onset flow is used to determine the relative onset flow ( $U_{rel}$ ) and inflow angle ( $\phi$ ) to the blade at each position along the blade, shown by Equations 3-4.

$$\delta U_{rel}(t) = \sqrt{U_X^2 + (\Omega r - U_\Theta)^2} \quad (3)$$

$$\delta\phi(t) = \sin^{-1} \frac{U_X(t)}{U_{rel}(t)} \quad (4)$$

Where  $U_{rel}$  is the relative velocity to the blade which incorporates the longitudinal velocity,  $U_X$  and the components in the tangential direction,  $U_\Theta$  with the angular velocity  $\omega$  and each radius  $r$ . The lift and drag force on each blade segment vary according to Equations 5-6.

$$\delta L(t) = \frac{1}{2} B \rho c (U_{rel})^2 C_L \delta r \quad (5)$$

$$\delta D(t) = \frac{1}{2} B \rho c (U_{rel})^2 C_D \delta r \quad (6)$$

Where  $c$  is the chord length,  $\delta r$  is the radial width of the blade segment,  $B$  is the number of blades,  $\rho$  is the fluid density,  $C_L$  and  $C_D$  correspond to the lift and drag coefficients respectively. Using the calculated lift and drag forces for each blade the axial ( $F_a$ ) and tangential ( $F_t$ ) forces along each blade are calculated using Equations 7-8.

$$\delta F_a(t) = \delta L(t) \cos(\phi(t)) + \delta D(t) \sin(\phi(t)) \quad (7)$$

$$\delta F_t(t) = \delta L(t) \sin(\phi(t)) - \delta D(t) \cos(\phi(t)) \quad (8)$$

The main interest here is the axial force ( $F_a$ ) on each segment of the blade as this leads to the calculation of root bending moment as well as rotor thrust. Both of these results can be used to establish the respective load spectra and hence determine the load cycles enabling the fatigue loads to be predicted.

#### B. Quantifying Fatigue Loads

Fatigue Loads are quantified in this study through the use of Damage Equivalent Loads (DEL). The values are determined by calculating the load cycles which are produced as the turbine rotates through different unsteady loading conditions, these conditions will be defined in Section III-C. Due to the unsteady nature of the loading, the best method to determine the load cycles is the Rainflow Cycle Counting method [17]. This method enables the determination of cycles for variable amplitude loading. It examines the tensile and compressive peaks within the time history of loading and calculates the ranges between successive tensile or compressive peaks depending on whether the following peak is less than or greater than the previous peak. These ranges are considered as 'half' cycles and are summated to determine the total number of cycles. This method has been applied to determine fatigue loads for offshore components in [18], [7].

The DELs are derived from a time history of loads using linear damage hypothesis to determine a single magnitude load repeating at a single frequency which would cause the same damage. Equation 9 defines damage equivalent loads, these are calculated using the number of cycles from the time history of loading.

$$L_m = \left( \frac{\sum_i n_i L_i^m}{fT} \right)^{1/m} \quad (9)$$

Where  $n_i$  is the number of cycles at each binned load magnitude  $m$  is the material gradient  $f$  is the repetition frequency  $T$  is the time sample length  $L_i$  is the load bin and  $L_m$  is the damage equivalent load for a given material gradient.

### C. Operational Conditions

The variation of disk averaged velocity for the turbine at this location is shown in Figure 2, as a histogram of the velocity samples for a turbine location near surface and near bed. Three onset flow points are considered which approximately represent below rated, rated and above rated power for a full scale turbine. For both tidal directions the flow is modelled to approach the turbine with 0deg offset. Realistically the flow does not oscillate between flood and ebb with exactly the same direction. The number of samples calculated for the flow speed bins will inform the calculation of damage equivalent loads to give a sample time over which the loads operate.

1) *Turbulence Modelling*: In order to model the loads experienced on the turbine in this method a frozen turbulence field is used as inflow. This field has been generated using the NREL Turbsim software, with a pre-defined variation of lengthscale and turbulence intensity. For the different turbine positions the turbulence characteristics have been calculated from the ADCP measurements at hub height. The von Kármán turbulence generation method is used here to synthesise the inflow with the length-scales determined through the use of auto-correlation at the hub height. From the ADCP measurements the average calculated integral lengthscales are given in Table III.

TABLE III  
HUB HEIGHT INTEGRAL LENGTHSCALES CALCULATED FROM MEASURED DATA FOR THREE DIFFERENT FLOW SPEED BINS.

Turbine Position	Integral Lengthscales (m) @ $U_{DA}$ (m/s)		
	1.8-2.0	2.2-2.4	2.6-2.8
Top	13.43	13.73	14.36
Bottom	14.41	14.92	15.53

For the top turbine position a lengthscale of 13.3 m is generated which falls within 8% of the lengthscales for each case. For the bottom case an integral lengthscale of 14.45 m is calculated, which is within 7% of the measured cases.

The turbulence intensity value used in the generation of the von Kármán turbulence field is taken from the fluctuation intensity values from the measured ADCP data. Figure 3 shows the fluctuation as the variation from the measured ADCP data at the hub height across a range of binned disk averaged velocities. For the two different hub heights there is a different range of intensity found, with the top hub height seeing a larger range of intensity. This is expected as any additional variation in intensity due to wave affects will be captured by the higher hub height rather than the lower hub height. The impact of the increased fluctuations on the fatigue loads is investigated. For both locations the top turbine position has a larger

mean fluctuation, this is expected with the interference caused by waves on the velocity fluctuations near the surface.

Following on from Table II, both the variation and mean fluctuation intensity have been used to determine their influence on the fatigue loads.

2) *Shear Flow*: Using a results from an ADCP allows a depth variation of velocity at a single location to be measured. This has enabled analysis of the turbines at varying heights. It also allows better understanding of the unsteady loading that the turbine could experience. It is generally understood that at most tidal sites a shear profile is present in the onset flow, a power law profile is commonly used, work by [19] shows that a 1/7th power law profile can adequately describe the shear. The variation in shear from the measurements is used for each of the onset flows considered, this is compared to a series of predicted profiles. These predicted profiles are calculated based upon a multi-parameter model to predict the variation of shear at the tidal site. These parameters have been defined in [2] which have been calibrated the values to the measurements from the EMEC test site as part of the ReDAPT project. Where a MIKE3 model was used to model the EMEC test site in the Fall of Warness, UK. This model was validated using current speed and direction, water depth and vertical shear profiles. It was found during this work that although a power law closely followed the vertical variation in the flood tide it did not capture the more complex flow variation in the ebb tide. Therefore in order to predict the profiles, a quadratic was fitted and the coefficients mapped out in [2]. This approach has been taken here to predict the shear profiles for both the flood and ebb tides.

## IV. FINDINGS

### A. Shear Variation

Using three different disk averaged velocities the variation in shear profile with position is determined. For the near surface turbine the measured shear profiles, shown in Figure 4 follow a consistent trend across all three flow speeds. For the ebb tide the measured profiles show a reverse shear across the top third of the disk, which is not captured in the predicted profiles. For the flood tide there is less variation across the rotor disk compared to the ebb tide and both the measured and predicted follow a very similar trend.

For the near bed case, shown in Figure 5, both tides show a slightly greater variation across the disk, 10% variation compared to 8.5% for the near surface case. The ebb tide for the measured cases shows a more parabolic profile compared to the near surface case, which the predicted profiles do not follow as closely. The next section will evaluate the impact of the mean and varying profiles on the damage equivalent loads for the 2.2-2.4 m/s case.

### B. Spatial Variation

Using the variation in shear profiles for the 2.2-2.4 m/s case the damage equivalent loads are determined, following the outline of cases given in Table II. These

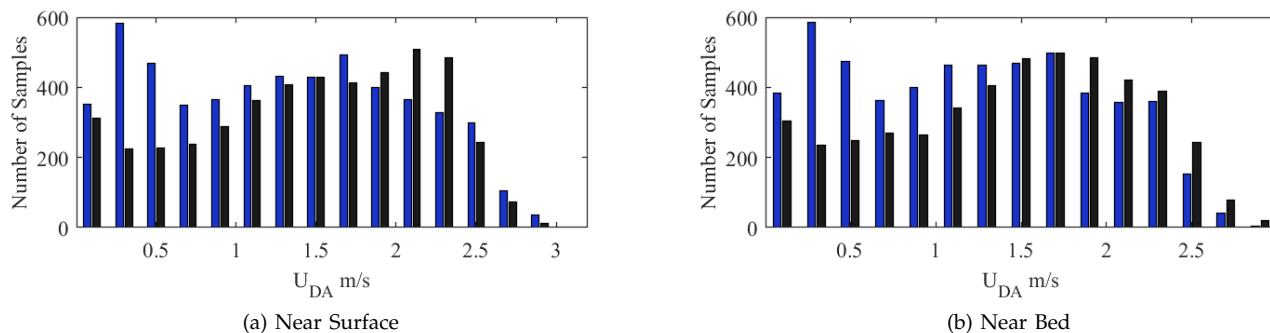


Fig. 2. Number of samples of disk averaged velocity at each hub height for the two turbine positions, for both tidal directions, flood (blue) and ebb (black).

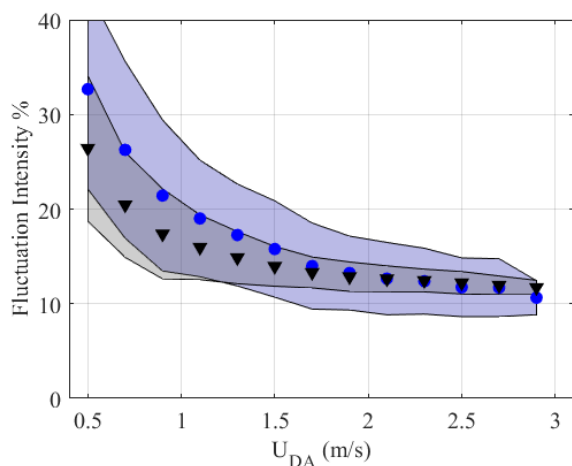


Fig. 3. Variation of fluctuation intensity at the hub height for each turbine position, Top turbine position (blue markers), Bottom turbine position (black markers). The shaded region represents the range of the intensity values at each  $U_{DA}$ .

loads are calculated for both turbine positions. The initial comparison shown in Figure 6 shows Cases A and C for a turbine blade experiencing varying turbulence intensity (TI). In this study the TI value is calculated as fluctuation intensity. All loads have been normalised by the maximum load calculated for the chosen flow speed, which is for the near surface turbine with flood tide and varying measured profiles.

Figure 6 shows greater loads are calculated for the near surface turbine. This is expected as the varying turbulence is greater for the near surface case, due to the inclusion of the influence of waves. The DEL for the near surface case with the flood tide are within 1.2% between the varying measured shear and the mean predicted profile. For the ebb tide there is a larger difference with the mean predicted loads 4.6% lower than the measured varying case. This is due to difference in the shape of the shear profile between the measured and predicted cases and is consistent with the larger variation in loads shown for the near bed case. For the flood tide with the near bed case there is a 3% variation in load, with the varying profiles providing lower loads. For the ebb tide with the near bed turbine the mean profiles also provide greater loads, but a greater difference in the mean loads of

TABLE IV  
COMPARISON OF DEL FROM VARYING MEASURED PROFILES TO THE DEL FROM APPLYING CONSTANT TURBULENCE WITH MEAN PREDICTED SHEAR.

Profiles Measured Varying with...	Near Surface Flood	Near Surface Ebb	Near bed Flood	Near bed Ebb
Varying Turbulence	18.4%	16.2%	0.7%	0.2%
Constant Turbulence	0%	0.3%	2.2%	1.8%

5%. Whereas for the near bed turbine in the flood tide the loads are within 0.5%, which corresponds to the similarity in the mean profiles shown in Figure 5(b).

The loads determined for the measured varying turbulence are compared to the loads for constant turbulence values in Figure 7. For the near surface turbine all loads calculated with mean turbulence value are within 20% of the varying turbulence loads. The reduction in load is a direct result of the removal of the varying turbulence intensity. Using a constant turbulence value has resulted in the calculated DEL from the mean profiles to be within 0.5% of the varying profiles. For the flood tide the variation between the predicted and measured loads is consistent with the varying turbulence with loads within 1.2% of each other. For the ebb tide the difference between predicted and measured has reduced to 2.9% compared to the 4.6% for the varying turbulence case. For the near bed case when compared to the varying turbulence case there is less difference in the magnitude of the loads. Consistently the mean profiles provided a higher load value than the varying profiles. The constant turbulence has reduced the mean loads by 2% for both the flood and ebb tides. The comparison of the DEL from the mean predicted shear to the measured varying shear is given in Table IV.

From the table it is shown that by applying constant turbulence the load on the near surface turbine is predicted well using the a constant model profile. However with varying turbulence intensity applied to varying measured profiles this is not replicated. For the near bed turbine the comparison between the mean predicted with constant turbulence intensity and the measured profiles with varying turbulence intensity is less than 1% compared to the slightly greater difference to the constant turbulence case.

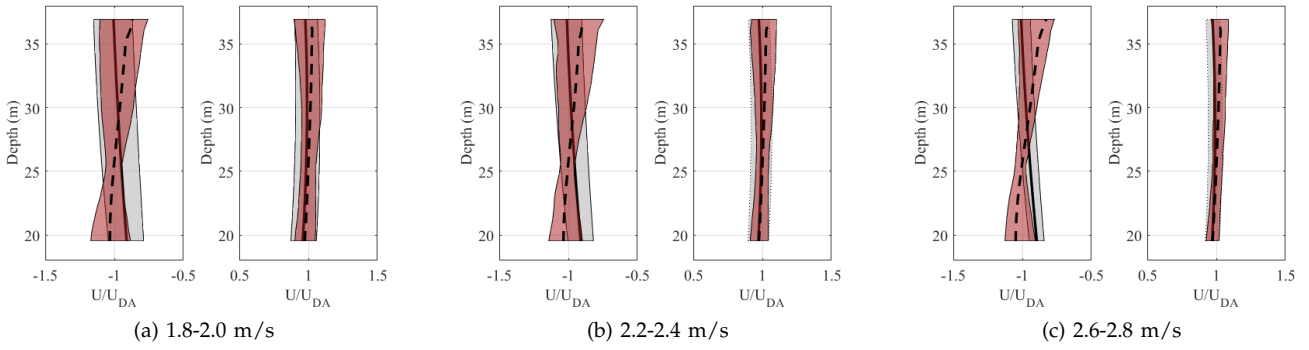


Fig. 4. For the near surface position, a range of shear profiles for three different disk averaged velocities, for varying measured profiles (red band), varying predicted profiles (grey band), mean measured (dashed black) and mean predicted (solid black).

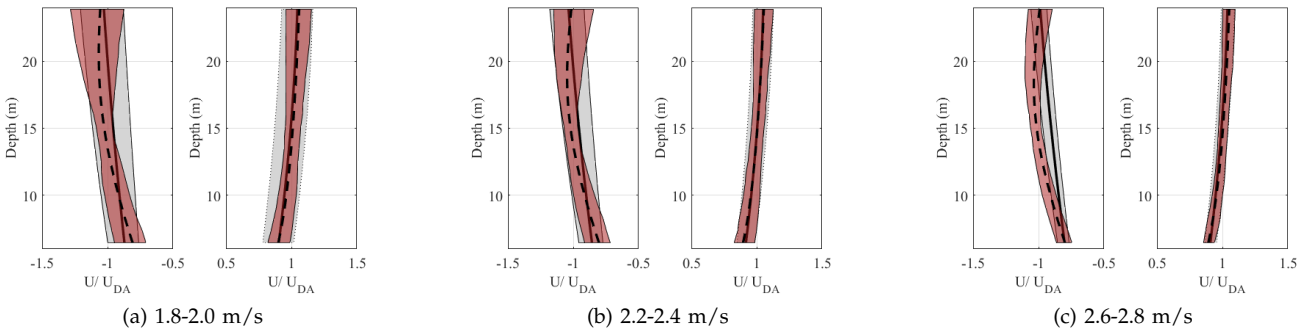


Fig. 5. For the near bed position, a range of shear profiles for three different disk averaged velocities, for varying measured profiles (red band), varying predicted profiles (grey band), mean measured (dashed black) and mean predicted (solid black).

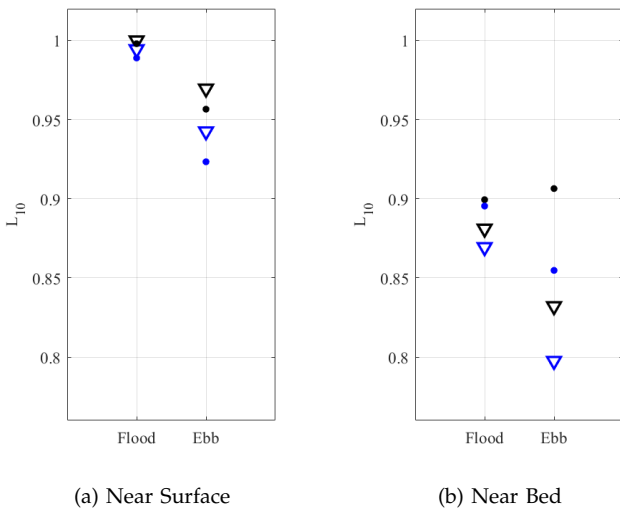


Fig. 6. Normalised damage equivalent loads for one velocity bin (2.2-2.4 m/s) determined using varying (open triangle) and mean (solid dot) measured profiles (black) and predicted profiles (blue).

C. Application to a tidal cycle

To consider long term loading the modelling has been expanded to include the range of flow speeds the turbine could experience. For each turbine position the range of disk averaged velocity is calculated based upon the measured samples. The range of samples found for each tide is shown in Figure 2. To study the range in damage equivalent loads the mean pre-

dicted profiles for each flow speed case are used. In addition to the mean profiles, a constant turbulence value is used for each velocity bin. The load cycles are determined per flow speed and increased to account for occurrence of the flow speed within the overall sample. The percentage occurrence is given in Figure 8 for the near-surface and near-bed turbine positions for the ebb tide. The ebb tide is shown as it has the largest variation in profile across the turbine. The damage equivalent loads shown here are normalised to the same value as the previous results (near-surface Case A for the flood tide), for consistency. In all cases the repetition frequency used to determine the damage equivalent loads are the same for all flow speeds, to allow for comparison.

Both turbine positions show an increase in DEL with flow speed until higher flow speeds, for the near surface turbine this then decreases at the highest  $U_{DA}$  found, for this case very few samples were used. The load cycles determined from the predicted mean profiles are aggregated to provide a DEL value for each turbine position. These load values have been normalised and are shown in Table V.

These aggregated load values are calculated based upon the mean predicted profiles for each tide, at each flow speed bin, with a representative number of load cycles calculated based on the sample size. For comparison, the DEL from the varying measured profiles with varying turbulence are shown in Figure 9, which correspond to the previous shear profiles shown. Following the DEL variation shown in Figure 7, the

TABLE V  
NORMALISED DAMAGE EQUIVALENT LOAD VALUES, USING THE MEAN PREDICTED PROFILES, DETERMINED USING AGGREGATE LOAD CYCLES FOR EACH FLOW SPEED WITH CONSTANT TURBULENCE.

	Flood	Ebb	Both
Near Surface	0.76	0.72	0.74
Near Bed	0.78	0.81	0.79

additional flow speeds follow the same trend with the near surface case showing greater DELs than the predicted values and the near bed at approximately the same magnitude. In order to calculate the aggregate loads from the measured varying case the difference in load cycles is found as a ratio which can be applied to the load cycles calculated for the predicted case, this variation is also shown in Figure 9.

The estimated DEL for the measured case allows for the calculation of the aggregated loads shown in Table VI. As expected the larger ratio is required to increase the load cycles for the near surface case, which results in an aggregated load 18-20% greater than the DEL calculated with the mean predicted shear. The difference in load cycles is a result of the greater variation in turbulence intensity. For the near bed case the load cycles from the measured varying case have approximately the same magnitude as the predicted mean case and therefore the measured DEL follow the same magnitude as the DEL from the predicted mean case. This has resulted in aggregated loads from the measured varying case which are within 1% of the predicted mean. With the loads determined across both tidal cycles 2% different for the near bed case and 19% for the near surface, consistent with the variation between tides.

However, a full comparison of loads across the tidal cycles can be made using the measured varying shear profiles and varying turbulence to the estimated

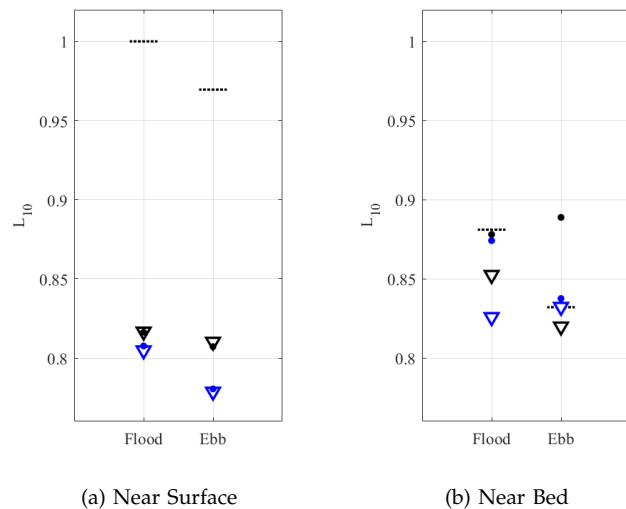


Fig. 7. Normalised damage equivalent loads for one velocity bin (2.2-2.4 m/s) determined using varying (open triangle) and mean (solid dot) measured profiles (black) and predicted profiles (blue) using a constant value for the fluctuation intensity, dashed lines to represent the measured varying case with varying fluctuation intensity.

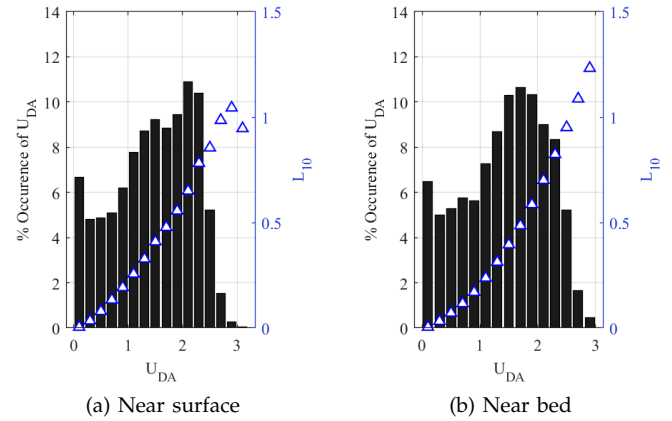


Fig. 8. Normalised damage equivalent loads for one velocity bin varying and mean measured profiles and predicted profiles, with constant mean fluctuation intensity (a) for the near-surface turbine position, (b) for the near-bed turbine position, dashed lines to represent the measured varying case with varying fluctuation intensity.

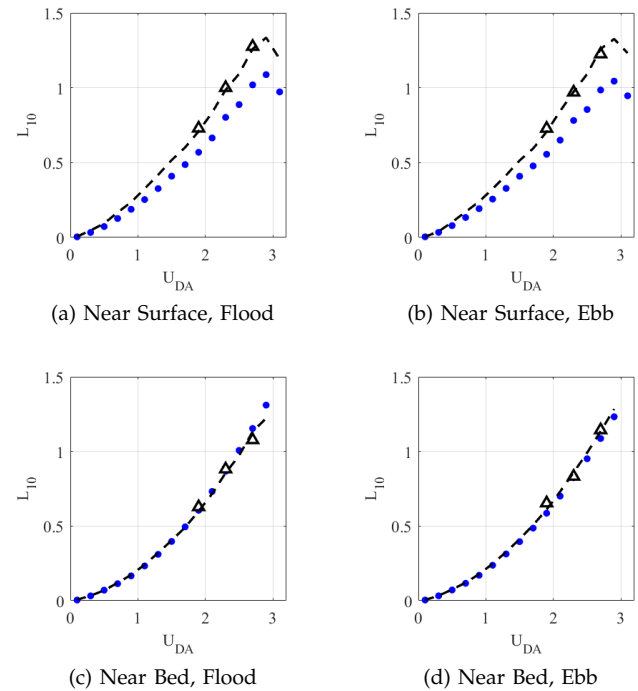


Fig. 9. Normalised DEL for the range of flow speeds for each turbine position and tide. Predicted mean profiles and constant turbulence (blue dot), Measured varying profiles and turbulence (black triangle), estimated loads from measured varying profiles (black dash).

loading, with the near surface turbine producing a normalised DEL of 0.92 and the near bed a normalised DEL of 0.82. These values are within 1% of the loads estimated using an increase in load cycles on the mean predicted case. For the near bed turbine the mean predicted case provides loads within 3% of when compared to the loading from the fully varying measured case and 18% greater for the near surface, which has a greater influence of the varying fluctuation intensity on the measured varying case.

## V. DISCUSSION

The comparison in damage equivalent loads between the near-surface and near-bed turbine may be accentuated

TABLE VI

ESTIMATE OF NORMALISED DAMAGE EQUIVALENT LOAD VALUES FOR MEASURED LOADS AT DIFFERENT ONSET FLOW SPEEDS, USING A RATIO BETWEEN RESULTS FROM VARYING MEASURED CASES WITH VARY TURBULENCE AND THE MEAN PREDICTED WITH CONSTANT TURBULENCE.

	Flood	Ebb	Both
Near Surface	0.94	0.92	0.93
Near Bed	0.77	0.82	0.81

ated by the use of the measured fluctuation intensity in the turbulent flow field set up. Due to the depth decay of turbulent kinetic energy caused by waves, they are not expected to contribute to the variation in velocity experienced by the near-bed turbine. This is shown through the similarities of the load values for the near bed turbine between varying and constant turbulence. Considering the lack of impact of external factors on the varying turbulence intensity of the near bed turbine, the predicted profiles are found to allow loads to be calculated to within 1% of the measured varying case. To reduce the difference in the loads at the near surface turbine the influence of the waves on the velocity fluctuations needs to be taken into account.

The predicted shear profiles used here from the multi-parameter model [2], do not specify different turbulence characteristics. These profiles have also been calibrated against the results from the ReDAPT project, although they show a better prediction for this site than a standard power law profile, this profile may not be a best representation of other tidal sites. To fully understand a site vertical shear profiles would be needed to validate model profiles.

Aggregated loads have been determined using a range of  $U_{DA}$  for the five tidal cycles. With the magnitude of the DELs from the measured varying case calculated based upon an increase in the load cycles across all flow speeds, to match the actual loads calculated from the measured varying at three flow speeds. The difference in aggregated DEL from the two methods is found to match the same variation found for the calculated DEL for the single flow speed shown in Figure 7, although of a smaller magnitude.

## VI. CONCLUSIONS

This study looked to establish the dependency of fatigue loads on the onset unsteady conditions obtained from shallow water models relative to ADCP measurement. A multi-parameter model is used to represent velocity profiles at the site for a range of disc averaged velocities. This combined with constant turbulence, synthesised with a von Karman spectral method, provides turbine fatigue loads to within 1% of the same loads obtained for all measured profiles of velocity and turbulence for the same disc-averaged velocity. Predictions are less accurate for a near-surface turbine location due to greater variation of measured turbulence, not captured by this approach. To account for the variation of turbulence, a scaling factor is applied to the load cycles for each disc averaged velocity, providing an estimate for both locations of

the aggregated damage equivalent loads across all flow conditions. This approach enables efficient prediction of damage equivalent load accumulated over a range of flow conditions by drawing on understanding of fatigue loads from only a small number of velocity profiles obtained for specific values of disc averaged velocity.

## ACKNOWLEDGEMENT

Site data was provided by Dr Brian Sellar, University of Edinburgh, from work conducted in the ReDAPT project.

## REFERENCES

- [1] B. G. Sellar, G. Wakelam, D. R. Sutherland, D. M. Ingram, and V. Venugopal, "Characterisation of tidal flows at the european marine energy centre in the absence of ocean waves," *Energies*, vol. 11, no. 1, 2018.
- [2] K. Gunn and C. Stock-Williams, "Fall of Warness 3D model validation report," Tech. Rep., 2014.
- [3] DNV-GL, "DNV GL STANDARD: Tidal turbines," Tech. Rep., 2015.
- [4] D. Peacock, "Power Performance Assessment of Electricity Producing Tidal Energy Converters Commissioned by : IEC," no. Cd, 2011.
- [5] B. G. Sellar and D. R. Sutherland, "Tidal Energy Site Characterisation At the Fall of Warness , Emec , Uk Energy Technologies Institute Redapt Ma1001 (Md3.8)," vol. 1001, no. December, 2016. [Online]. Available: <http://redapt.eng.ed.ac.uk>
- [6] J. McNaughton, S. Harper, R. Sinclair, B. Sellar, A. O. Energy, and F. Castlemead, "Measuring and Modelling the Power Curve of a Commercial-Scale Tidal Turbine," *Alstom*, 2015.
- [7] S. G. Parkinson and W. J. Collier, "Model validation of hydrodynamic loads and performance of a full-scale tidal turbine using Tidal Bladed," *International Journal of Marine Energy*, vol. 16, pp. 279–297, 2016. [Online]. Available: <http://dx.doi.org/10.1016/j.ijome.2016.08.001>
- [8] G. N. McCann, R. I. Rawlinson-smith, and K. Argyriadis, "Load Simulation for Tidal Turbines using Wind Turbine Experience," *GH Tidal Bladed*, no. 1870, p. 10, 2007.
- [9] I. a. Milne, R. N. Sharma, R. G. J. Flay, and S. Bickerton, "The Role of Onset Turbulence on Tidal Turbine Blade Loads," in *17th Australasian Fluid Mechanics Conference Auckland New Zealand 59 December 2010*, no. December, 2010, pp. 1–8.
- [10] J. McNaughton, S. Harper, R. Sinclair, and B. Sellar, "Measuring and Modelling the Power Curve of a Commercial-Scale Tidal Turbine," in *Proceedings of 11th European Wave and Tidal Energy Conference, Nantes, France*, vol. 1, 2015, pp. 1–9.
- [11] D. R. J. Sutherland, B. G. Sellar, V. Venugopal, and A. G. L. Borthwick, "Effects of Spatial Variation and Surface Waves on Tidal Site Characterisation," pp. 1–8, 2017.
- [12] a. Olczak, T. Stallard, T. Feng, and P. K. Stansby, "Comparison of a RANS blade element model for tidal turbine arrays with laboratory scale measurements of wake velocity and rotor thrust," *Journal of Fluids and Structures*, vol. 64, pp. 87–106, 2016. [Online]. Available: <http://dx.doi.org/10.1016/j.jfluidstructs.2016.04.001>
- [13] D. D. Apsley, T. Stallard, and P. K. Stansby, "Actuator-line CFD modelling of tidal-stream turbines in arrays," *Journal of Ocean Engineering and Marine Energy*, 2018. [Online]. Available: <http://link.springer.com/10.1007/s40722-018-0120-3>
- [14] U. Ahmed, D. Apsley, I. Afghan, T. Stallard, and S. P.K., "Fluctuating Loads on a Tidal Turbine Due to Velocity Shear and Turbulence: Comparison of CFD with Field Data." *Renewable Energy*, pp. 235–246, 2017.
- [15] H. R. Mullings and T. Stallard, "Assessment of tidal turbine load cycles using synthesised load spectra , including blade-scale fluctuations," pp. 1–9, 2019.
- [16] H. Mullings, "Operational Loads On A Tidal Turbine," Ph.D. dissertation, 2019.
- [17] S. D. Downing and D. F. Socie, "Simple rainflow counting algorithms," *International Journal of Fatigue*, vol. 4, no. 1, pp. 31–40, 1982.
- [18] S. D. Weller, P. R. Thies, T. Gordelier, and L. Johanning, "Reducing Reliability Uncertainties for Marine Renewable Energy," *Journal of Marine Science and Engineering*, vol. 3, pp. 1349–1361, 2015.

- [19] M. Togneri, I. Masters, and J. Orme, "Incorporating Turbulent Inflow Conditions in a Blade Element Momentum Model of Tidal Stream Turbines," in *Proceedings of the Twenty-first (2011) International Offshore and Polar Engineering Conference*, vol. 8, 2011, pp. 757-762.